Eur. Phys. J. D **27**, 55–72 (2003)
DOI: 10.1140/epjd/e2003-00227-1

THE EUROPEAN PHYSICAL JOURNAL D

Comparison of different techniques for the FLUENT©-based treatment of the electromagnetic field in inductively coupled plasma torches

D. Bernardi, V. Colombo[a], E. Ghedini, and A. Mentrelli

Università degli Studi di Bologna, Dipartimento di Ingegneria delle Costruzioni Meccaniche, Nucleari, Aeronautiche e di Metallurgia (D.I.E.M.) and C.I.R.A.M., Via Saragozza 8, 40123 Bologna, Italy

Received 21 February 2003
Published online 29 July 2003 – © EDP Sciences, Società Italiana di Fisica, Springer-Verlag 2003

Abstract. A new technique for using the CFD commercial code FLUENT© to simulate inductively coupled plasma torches by means of two-dimensional axisymmetric models is presented. The method is based on an external user-defined function (UDF) which fully solves the electromagnetic field equations, letting the FLUENT© built-in module calculate only the plasma temperature and velocity fields inside the torch region. In this framework, computations have been carried out for LTE, optically thin argon plasmas at atmospheric pressure, using extended grid models with either magnetic dipole or vanishing vector potential boundary conditions for the electromagnetic field. It is shown that our newly developed technique is up to 60% faster on each iteration than that using user-defined scalars (UDS) previously proposed in the literature, as the need of solving flow field equations also outside the plasma zone is eliminated. Calculations are also performed using exact integral boundary conditions for the vector potential, as given by the standard electromagnetic field approach, taking into account the effects of both exciting and induced currents. The corresponding results are compared with the approximate ones obtained by employing extended grid models, showing that for small radial dimensions of the electromagnetic field domain, the magnetic dipole boundary conditions give more realistic solutions than those assuming a vanishing vector potential.

PACS. 52.75.Hn Plasma torches – 52.65.-y Plasma simulation – 52.80.Pi High-frequency and RF discharges

1 Introduction

Mathematical modelling is a powerful tool to deeply investigate physical and chemical phenomena occurring within inductively coupled plasma torches (ICPTs). Various numerical models of increasing complexity have been proposed over the years with the aim of obtaining a more and more realistic prediction of plasma behaviour and chemical processes inside the torch. Current state of the art in this research field includes the fully 3-D description of the system, as recently performed by the authors by means of either complete [1] or simplified [2] approaches for the treatment of the electromagnetic field.

Nevertheless, two-dimensional axisymmetric models are still widely used for calculating the plasma temperature, flow and concentration fields in ICPTs. In this regard, many efforts have been devoted in the last years to continuously improve 2-D models, *e.g.* by taking into account also turbulence phenomena [3] or including some important 3-D effects due to the non-axisymmetric shape of the induction coil [4].

Besides this, special care has been dedicated to optimize the treatment of the electromagnetic (EM) field, which usually represents a critical task in the modelling of induction plasma torches. This is due to the fact that the standard (ST) vector potential formulation employed within most 2-D models [5–7] relies on the classic Biot-Savart integral boundary conditions, which introduce a strongly non linear coupling between the boundary values of the vector potential and the current density distribution induced in the plasma. As a consequence, an iterative approach must be adopted to solve the EM field equations, leading to slow convergence of the numerical procedure. In order to overcome this problem, it is possible to replace the ST formulation with more efficient approaches in which the computational domain for the EM field extends beyond the plasma discharge region and far field boundary conditions are adopted; in this frame, magnetic dipole boundary conditions (MDBC) have been proposed by some of the authors [8,9] as well as the employment of extended field (EF) vanishing conditions [4,10].

In addition to the improvement of 2-D models, much work has been done to suitably customize the CFD commercial code FLUENT© for simulating RF thermal

[a] e-mail: colombo@ciram.ing.unibo.it

plasma sources. FLUENT© offers important advantages in modelling, such as the possibility of studying complicated geometries, using different physical and numerical models and easily generating both structured and unstructured meshes. The need for customizing the basic code lies in the fact that, by default, the FLUENT© built-in solver can only treat mass, momentum and energy conservation equations, but it does not include any computational module for solving the electromagnetic field equations involved in the modelling of induction plasmas.

To overcome this difficulty, Boulos *et al.* [4,10] exploit the FLUENT© feature which allows one to add new user-defined scalars (UDS) to the variables basically employed by the built-in solver. In particular, they define two UDS for the real and imaginary parts of the complex vector potential and then let the FLUENT© routines solve the corresponding governing equations. This approach is quite simple to implement but has some numerical drawbacks due to the intrinsic customization limits of the software. In fact, FLUENT© requires all the equations of the model to be solved on the same domain, which implies that even the computation of the fluid dynamic variables must be extended outside the torch region when a far field approach is used for the treatment of the electromagnetics of the system. This might result in numerical unstabilities and/or slow convergence of the solution process.

In this work, a new technique for the simulation of ICPTs within FLUENT© environment is presented. Following this technique, vector potential equations are fully solved by means of an external C user-defined function (UDF) developed by the authors, which is linked to the FLUENT© built-in code. In this way, the latter can be completely dedicated to solve only flow field equations in a domain restricted to the torch region.

In the present paper, results obtained by means of our new UDF technique will be presented, showing the effects of using ST, MDBC and EF approaches for the treatment of the EM field on the calculated plasma temperature, velocity and electromagnetic field distributions. Moreover, computations have been carried out using also the UDS technique in order to compare its performances with the ones of the new method proposed in this work.

2 Modelling approach

The following basic assumptions have been adopted throughout this work:

- the torch is represented by a fully axisymmetric configuration;
- the plasma is assumed to be optically thin and in local thermodynamic equilibrium (LTE) under atmospheric pressure conditions;
- the flow is laminar and the tangential component of plasma velocity is not taken into account;
- viscous dissipation and pressure work in the energy equation are neglected;
- displacement current associated with the oscillatory magnetic field is assumed to be negligible.

2.1 Electromagnetic field treatment

The electromagnetic field generated by the current density flowing through the coil, $\mathbf{J}_{\mathrm{coil}}$, and that induced in the plasma, $\mathbf{J}_{\mathrm{ind}}$, is governed by Maxwell's equations which, in our case, can be written as:

$$\nabla \cdot \mathbf{E} = 0 \tag{1}$$

$$\nabla \cdot \mathbf{B} = 0 \tag{2}$$

$$\nabla \times \mathbf{E} = -\frac{\partial \mathbf{B}}{\partial t} \tag{3}$$

$$\nabla \times \mathbf{B} = \mu_0(\mathbf{J}_{\mathrm{coil}} + \mathbf{J}_{\mathrm{ind}}) \tag{4}$$

where $\mathbf{E}$ and $\mathbf{B}$ are the electric and magnetic field intensities, respectively, and μ_0 is the permeability of the free space. The displacement current density is considered negligible as compared to the conductive one, since for the current frequency and torch geometry considered here, the wavelength of the EM field is much greater than the characteristic dimensions of the torch. Moreover, according to the *quasi-neutrality* property of plasmas, the electric charge density is supposed to be zero everywhere. For our purposes, it is convenient to introduce the magnetic vector potential, $\mathbf{A}$, which is defined by:

$$\mathbf{B} = \nabla \times \mathbf{A}. \tag{5}$$

Using expression (5) in equation (3) and considering that in the absence of electrostatic fields the scalar potential vanishes, we obtain the relation between $\mathbf{A}$ and $\mathbf{E}$:

$$\mathbf{E} = -\frac{\partial \mathbf{A}}{\partial t}. \tag{6}$$

Inserting equation (5) into (4) and making use of the identity:

$$\nabla \times \nabla \times \mathbf{A} \equiv -\nabla^2 \mathbf{A} + \nabla(\nabla \cdot \mathbf{A}) \tag{7}$$

we obtain, by means of the Coulomb gauge, $\nabla \cdot \mathbf{A} = 0$:

$$\nabla^2 \mathbf{A} = -\mu_0(\mathbf{J}_{\mathrm{coil}} + \mathbf{J}_{\mathrm{ind}}). \tag{8}$$

The induced current density, $\mathbf{J}_{\mathrm{ind}}$, can be expressed by simplified Ohm law:

$$\mathbf{J}_{\mathrm{ind}} = \sigma \mathbf{E} = -\sigma \frac{\partial \mathbf{A}}{\partial t} \tag{9}$$

where σ is the temperature-dependent electric conductivity of the plasma. Hence, equation (8) can be written as:

$$\nabla^2 \mathbf{A} - \mu_0 \sigma \frac{\partial \mathbf{A}}{\partial t} = -\mu_0 \mathbf{J}_{\mathrm{coil}}. \tag{10}$$

Assuming that both $\mathbf{J}_{\mathrm{coil}}$ and $\mathbf{A}$ are characterized by a sinusoidal time variation with frequency f, the classic complex notation can be used to eliminate the time variable in equation (10). To do so, we express $\mathbf{J}_{\mathrm{coil}}$ and $\mathbf{A}$ as:

$$\mathbf{J}_{\mathrm{coil}}(\mathbf{r}, t) = \Re\left[\widetilde{\mathbf{J}}_{\mathrm{coil}}(\mathbf{r}) \mathrm{e}^{\mathrm{i}\omega t}\right] \tag{11}$$

$$\mathbf{A}(\mathbf{r}, t) = \Re\left[\widetilde{\mathbf{A}}(\mathbf{r}) \mathrm{e}^{\mathrm{i}\omega t}\right] \tag{12}$$

where $\widetilde{\mathbf{J}}_{\rm coil}$ and $\widetilde{\mathbf{A}}$ represents the corresponding phasors and $\omega = 2\pi f$. Using expressions (11, 12), equation (10) becomes:

$$\nabla^2 \widetilde{\mathbf{A}} - \mathrm{i}\mu_0\sigma\omega\widetilde{\mathbf{A}} = -\mu_0\widetilde{\mathbf{J}}_{\rm coil}. \quad (13)$$

Under the assumption of axisymmetric configuration for the induction circuit, the electric current density flowing in the coil and, consequently, the magnetic vector potential, will only have tangential components, *i.e.*:

$$\widetilde{\mathbf{J}}_{\rm coil} = (0, J_{\rm coil}, 0) \quad (14)$$

$$\widetilde{\mathbf{A}} = (0, A_\theta, 0) \quad (15)$$

and thus equation (13) reduces to:

$$\frac{1}{r}\frac{\partial}{\partial r}\left(r\frac{\partial A_\theta}{\partial r}\right) + \frac{\partial^2 A_\theta}{\partial z^2} - \left(\frac{A_\theta}{r^2} + \mathrm{i}\mu_0\sigma\omega A_\theta\right) = -\mu_0 J_{\rm coil}. \quad (16)$$

Writing A_θ by means of its real and imaginary components, $A_{\theta \rm r}$ and $A_{\theta \rm i}$:

$$A_\theta = A_{\theta \rm r} + \mathrm{i}A_{\theta \rm i}$$

equation (16) can be split into the followings:

$$\frac{1}{r}\frac{\partial}{\partial r}\left(r\frac{\partial A_{\theta \rm r}}{\partial r}\right) + \frac{\partial^2 A_{\theta \rm r}}{\partial z^2} - \frac{A_{\theta \rm r}}{r^2} + \mu_0\sigma\omega A_{\theta \rm i} = -\mu_0 J_{\rm coil} \quad (17)$$

$$\frac{1}{r}\frac{\partial}{\partial r}\left(r\frac{\partial A_{\theta \rm i}}{\partial r}\right) + \frac{\partial^2 A_{\theta \rm i}}{\partial z^2} - \frac{A_{\theta \rm i}}{r^2} - \mu_0\sigma\omega A_{\theta \rm r} = 0. \quad (18)$$

Provided that $J_{\rm coil}$ is given, equations (17, 18) can be solved to calculate the vector potential. Once the latter is known, relations (5, 6) are used to obtain the components of the magnetic and electric fields, which are given by:

$$B_z = \frac{1}{r}\frac{\partial}{\partial r}(rA_\theta) \quad (19)$$

$$B_r = -\frac{\partial}{\partial r}(A_\theta) \quad (20)$$

$$E_\theta = -\mathrm{i}\omega A_\theta. \quad (21)$$

Various methods differing in terms of type of computational grid and boundary conditions, can be adopted to solve equations (17, 18).

In this work, both the MDBC [8] and EF [10] far field approaches, along with the ST model formulation [5], have been considered. For the sake of clarity, a brief review of these methods is given in the following sections.

2.1.1 ST approach

The ST approach assumes that the computational domain for the EM field calculations is limited only to the plasma region (*i.e.*, to the zone defined by $0 \le r \le R_0$; $0 \le z \le L_T$, see Fig. 1). Since no excitation currents are present in this region, equations (17, 18) with $J_{\rm coil} = 0$

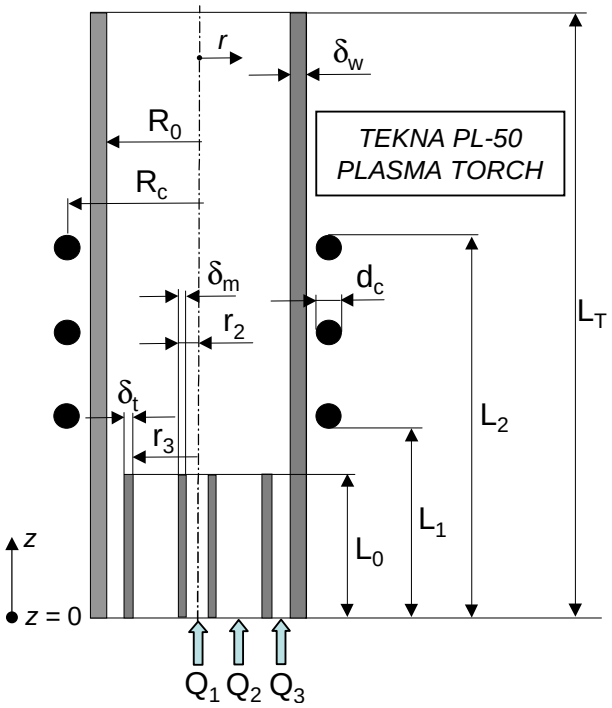

Fig. 1. Schematic of the plasma torch.

are used to calculate the vector potential. According to the axisymmetry hypothesis, the vanishing condition:

$$A_\theta(0, z) = 0 \quad (22)$$

is set on the axis of the torch, while at the other boundaries of the domain the values of A_θ can be obtained using the well-known formula of the single current-carrying loop [11], summing up all the contributions coming from both excitation and induced currents flowing in the coil and in the plasma, respectively. To numerically solve equations (17, 18), the plasma region is to be divided into $N_{\rm cv}$ cylindrical control volumes and the vector potential in each point (R_b, Z_b) of the boundaries can be expressed as:

$$A_\theta(R_b, Z_b) = -\frac{\mathrm{i}\omega\mu_0}{2\pi}\sum_{j=1}^{N_{\rm cv}}(\sigma_j A_{\theta j})\Delta S_j\sqrt{\frac{r_j}{R_b}}G(k_j) + \frac{\mu_0 I_{\rm c}}{2\pi}\sum_{i=1}^{N_{\rm c}}\sqrt{\frac{R_i}{R_b}}G(k_i) \quad (23)$$

where the quantity $(-\mathrm{i}\omega\sigma_j A_{\theta j})\Delta S_j$ in the first summation in the right-hand side of equation (23) represents the induced current flowing through the cross-section, ΔS_j, of the jth control volume, located at the point (r_j, z_j), while the second summation extends over the $N_{\rm c}$ cylindrical loops of radius R_i and height Z_i, in which the coil region is discretized. Assuming a uniform distribution of the current density in the coil, the current, $I_{\rm c}$, flowing through the cross-section of each loop, $\Delta S_{\rm t}$, can be expressed as: $I_{\rm c} = J_{\rm coil}\Delta S_{\rm t}$. The function $G(k)$ in equation (23) is

given by:

$$G(k) = \frac{\left(2-k^2\right)K(k) - 2E(k)}{k} \tag{24}$$

being K and E the elliptic integrals of first and second kind, respectively, and

$$k_j = \left[\frac{4r_j R_b}{\left(r_j + R_b\right)^2 + \left(Z_b - z_j\right)^2}\right]^{\frac{1}{2}} \tag{25}$$

$$k_i = \left[\frac{4R_i R_b}{\left(R_i + R_b\right)^2 + \left(Z_b - Z_i\right)^2}\right]^{\frac{1}{2}}. \tag{26}$$

Boundary conditions (23) are rigorous, that is, they are derived analytically from equation (13). However, due to the term accounting for the effects of the induced currents, the whole distribution of A_θ in the plasma region needs to be known to determine the vector potential at each point on the boundaries. Thus, an iterative approach has to be employed to solve the electromagnetic field equations, leading to slow convergence of the numerical process. To overcome such difficulty, the contribution of the induced currents in equation (23) can be neglected with respect to that due to the coil. However, as in most cases this represents a quite drastic approximation, all the terms in (23) have been retained here.

2.1.2 MDBC approach

Unlike the ST method, the MDBC approach [8] uses a computational grid which extends well outside the plasma discharge region, so that simpler boundary conditions can be adopted for the vector potential. The electromagnetic field is calculated by solving equations (17, 18), setting $J_{\text{coil}} = 0$ everywhere except in the discretized coil region.

Boundary conditions are defined by assuming that, at the borders of the extended domain, the torch can be regarded as a single loop carrying a current equal to the sum of all the currents flowing in the plasma and in the coil. Namely, we suppose that, far enough away from the discharge, the whole system can be treated as a single magnetic dipole placed at the mid-coil point, with momentum parallel to the axis of the torch.

Under such an assumption and taking a cylindrical (r, z) reference frame with the origin at the dipole and z-axis parallel to its momentum, the vector potential at sufficient distance from the torch is given by the classic expression:

$$A_\theta = C\frac{r}{\left(r^2+z^2\right)^{\frac{3}{2}}} \tag{27}$$

where C is a constant which accounts for the momentum of the dipole, whose value is not known *a priori* as it depends upon the induced currents which, in turn, depend upon the vector potential in the discharge region. However, the value of C is not actually required for our purposes. In fact, taking the r-derivative of expression (27) and using the (27) itself, we obtain the relation:

$$\frac{\partial A_\theta}{\partial r} = \frac{\left[1 - 3r^2\left(r^2+z^2\right)^{-1}\right]}{r} A_\theta \tag{28}$$

which can be assumed as boundary condition for A_θ at the border $r = R_{\text{et}}$ (see Fig. 2) of the computational domain. Likewise, taking the z-derivative of (27), we have:

$$\frac{\partial A_\theta}{\partial z} = -\frac{3z}{r^2+z^2} A_\theta \tag{29}$$

which provides the boundary conditions to be set at the two borders of the extended domain located on planes perpendicular to the z-direction. Finally, on the axis of the torch, the axisymmetry condition (22) is imposed.

Expressions (28, 29) can be directly embedded into the discretized form of the vector potential equation. Therefore, in this case, no iterations on the boundary values are required to obtain A_θ. However, a numerical problem of bigger dimension has to be solved with respect to the ST approach, due to the wider domain employed for the EM field calculations.

2.1.3 EF approach

In this case, an extended grid similar to that adopted in the MDBC approach is used for the treatment of the EM field, but the following conditions:

$$A_\theta(R_b, Z_b) = 0 \tag{30}$$

corresponding to a vanishing value for A_θ at the outer boundaries of the EM field domain are applied instead of (28) and (29).

2.2 Fluid dynamic model

Fluid dynamic equations for the plasma are as follows:

– continuity:

$$\frac{1}{r}\frac{\partial}{\partial r}\left(r\rho v_r\right) + \frac{\partial}{\partial z}\left(\rho v_z\right) = 0; \tag{31}$$

– momentum:

$$\rho\left(v_r\frac{\partial v_r}{\partial r} + v_z\frac{\partial v_r}{\partial z}\right) = -\frac{\partial p}{\partial r} + \frac{2}{r}\frac{\partial}{\partial r}\left(\mu r\frac{\partial v_r}{\partial r}\right) + \frac{\partial}{\partial z}\left[\mu\left(\frac{\partial v_r}{\partial z} + \frac{\partial v_z}{\partial r}\right)\right] - \frac{2\mu v_r}{r^2} + F_r \tag{32}$$

$$\rho\left(v_r\frac{\partial v_z}{\partial r} + v_z\frac{\partial v_z}{\partial z}\right) = -\frac{\partial p}{\partial z} + 2\frac{\partial}{\partial z}\left(\mu\frac{\partial v_z}{\partial z}\right) + \frac{1}{r}\frac{\partial}{\partial r}\left[r\mu\left(\frac{\partial v_z}{\partial r} + \frac{\partial v_r}{\partial z}\right)\right] + F_z; \tag{33}$$

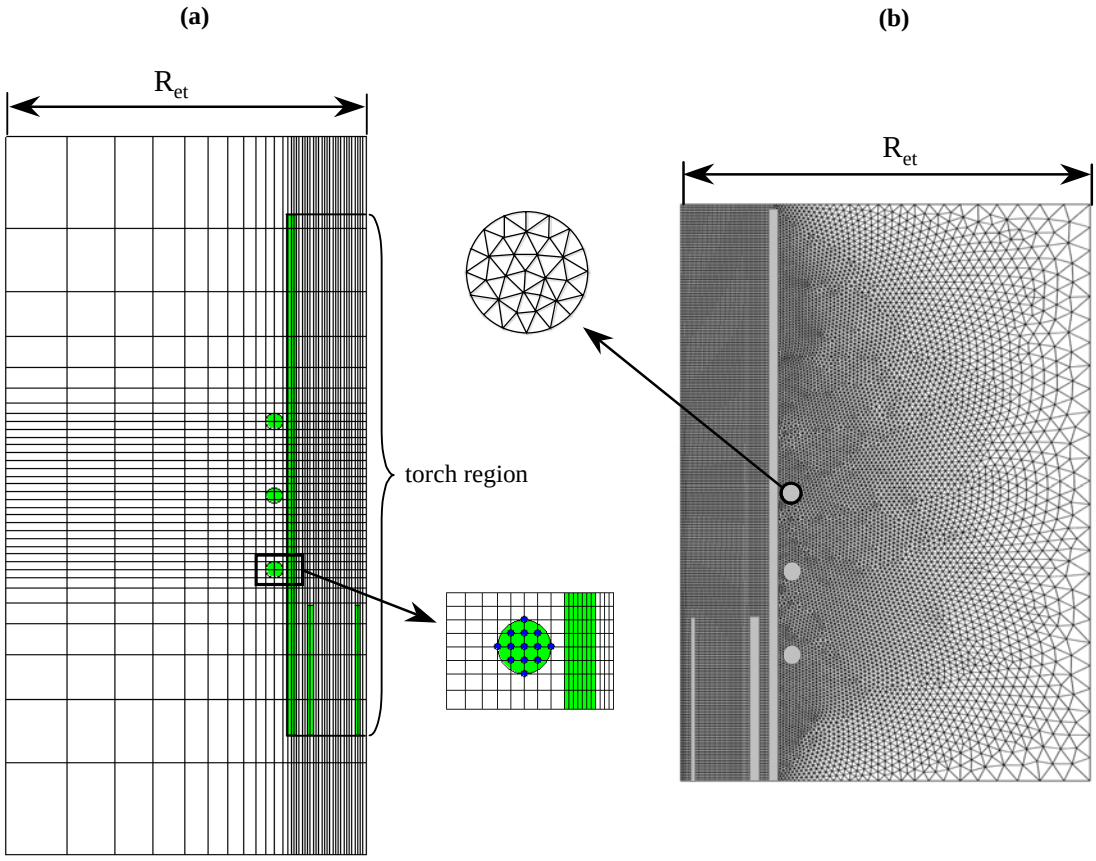

Fig. 2. Computational grids for the electromagnetic field and details of the coil discretization for (a) UDF and (b) UDS techniques.

– energy:

$$\rho\left(v_r\frac{\partial h}{\partial r}+v_z\frac{\partial h}{\partial z}\right)=\frac{1}{r}\frac{\partial}{\partial r}\left(r\frac{k}{c_p}\frac{\partial h}{\partial r}\right)+\frac{\partial}{\partial z}\left(\frac{k}{c_p}\frac{\partial h}{\partial z}\right)+Q_J-Q_R \quad (34)$$

where h is the plasma specific enthalpy; v_r, v_z are the radial and axial components of plasma velocity; ρ, k, μ, c_p are the density, thermal conductivity, viscosity and specific heat at constant pressure of the plasma, respectively; p is the pressure; Q_J and Q_R are the Joule heating rate and the plasma radiation losses per unit volume and F_r, F_z are the radial and axial components of the Lorentz force.

Since the characteristic time of variation of the plasma temperature and velocity is much longer than that of the EM field, the terms Q_J, F_r and F_z in the above equations can be expressed, by taking the average over one oscillation period, as:

$$Q_J=\frac{1}{2}\sigma\left|E_\theta\right|^2 \quad (35)$$

$$F_r=\frac{1}{2}\sigma\Re\left[E_\theta B_z^*\right] \quad (36)$$

$$F_z=-\frac{1}{2}\sigma\Re\left[E_\theta B_r^*\right] \quad (37)$$

where the superscript * denotes the complex conjugates.

The behaviour of the volumetric radiation losses as a function of plasma temperature, T, is supposed to be given by the classic relation adopted in [12], which assumes $Q_R=0$ when $T\leq 9500$ K and

$$Q_R=5600\left(T-9500\right)+181\left(T-9500\right)^2 \quad (38)$$

otherwise (T being expressed in K and Q_R in W/m^3).

Boundary conditions for the plasma temperature and velocity are the same used in [10].

3 Computational technique

In spite of many advantages offered by the FLUENT© code for studying complex fluid dynamic phenomena, its use in the modelling of inductive plasmas is not straightforward. This is due to the fact that, at present, FLUENT© solves, by default, only mass, momentum and energy conservation equations but does not provide any built-in module for EM field calculations. To overcome this difficulty, two different techniques exploiting FLUENT© customization capabilities can be followed.

The first technique, which has been proposed in [10], makes use of two user-defined scalar (UDS) variables for the real and imaginary parts of the complex vector potential, in addition to the ones basically employed by

Table 1. Torch dimensions and operating conditions.

$L_0 = 50$ mm	$r_2 = 3.7$ mm	$\delta m = 2$ mm	$Q_1 = 1$ slpm	$P = 5$ kW
$L_1 = 60$ mm	$r_3 = 18.8$ mm	$\delta t = 2.2$ mm	$Q_2 = 3$ slpm	$f = 3$ MHz
$L_2 = 124$ mm	$R_0 = 25$ mm	$\delta w = 3.5$ mm	$Q_3 = 31$ slpm	
$L_T = 200$ mm	$R_c = 33$ mm	$d_c = 6$ mm		

the FLUENT© solver, that is, temperature and velocity components of the fluid. For each generic UDS variable, ϕ, added to the basic model, FLUENT© automatically solves an extra conservation-like equation having the general form:

$$\nabla \cdot (\rho \mathbf{v} \phi) = \nabla \cdot (\Gamma_\phi \nabla \phi) + S_\phi \tag{39}$$

$\mathbf{v}$ being the fluid velocity, and Γ_ϕ, S_ϕ, to be specified by the user, the diffusion coefficient and the source term per unit volume, respectively. By suitably setting ϕ, Γ_ϕ and S_ϕ, it is easy to observe that equation (39) can reproduce both the real and imaginary parts of vector potential equation in all the zones of the computational domain. For example, in the plasma region, in which $J_{\mathrm{coil}} = 0$, equation (17) can be simply reproduced by taking $\phi = A_{\theta \mathrm{r}}$, $\Gamma_\phi = 1$ and $S_\phi = \mu_0 \sigma \omega A_{\theta \mathrm{i}}$.

Although quite simple to implement, the UDS technique is not the best way of using FLUENT© for treating the EM field. In fact, in the current version of the code, all governing equations are to be specified for the same computational domain. Besides, FLUENT© can solve UDS equations only inside fluid regions. This means that when the UDS technique is used in conjunction with the MDBC or EF approaches for the EM field calculations, fluid dynamic equations must be solved also outside the torch region, treating all zones of the domain as if they were occupied by a fluid. As a consequence, fictitious source terms must be introduced in the momentum and energy equations to obtain a zero velocity field in the regions where there is no plasma and to impose a constant temperature (a value of 300 K is assumed in this work) outside the plasma confinement tube [10]. This results in a somewhat "unnatural" use of the code, that slows down its convergence velocity and may cause numerical instabilities.

To better exploit the FLUENT© capabilities, a new technique has been developed in this work for the treatment of the EM field. This technique uses an external user-defined function (UDF) linked to the FLUENT© code, which completely solves the vector potential equations by means of a finite difference approach, while leaving to the FLUENT© solver the task of computing only the plasma temperature and velocity fields in the torch region. The electromagnetic field is calculated on a structured, orthogonal grid defined by the UDF, while flow field equations are solved on a different mesh generated by means of the FLUENT© pre-processor (GAMBIT©).

Each turn of the induction coil is modelled with a series of 13 current-carrying rings (see Fig. 2), assuming in it a uniform distribution of the current density, J_{coil}, so that: $J_{\mathrm{coil}} = I/S_{\mathrm{c}}$, being I the current flowing through the coil and S_{c} the cross section of a single turn.

Within the framework of the UDF technique, all three approaches described above for the EM field treatment (ST, MDBC and EF) have been implemented.

The UDF and the FLUENT© solver interact in the following manner: at each iteration, the UDF receives, as input data, the values of the plasma electric conductivity calculated by the FLUENT© solver and gives back to it the electric and magnetic field distributions inside the torch region. The calculated EM field is then used by the FLUENT© solver for updating the values of the Lorentz force and of the Joule heating rate in Navier-Stokes and energy equations. A suitable numerical routine has been developed, as a part of the UDF, with the purpose of interpolating input and output data from the electromagnetic grid to the fluid dynamic one and *vice versa*. Although this routine has been designed to work with both structured and unstructured fluid dynamic meshes, only structured grids with quadrilateral cells have been used in this work for the solution of flow field equations.

Since, in the UDF approach, the FLUENT© solver is used to calculate only temperature and velocity fields in a computational domain limited to the torch region, the above-mentioned drawbacks arising within the UDS technique are eliminated: in the new approach, all solid zones of the fluid dynamic domain (such as the plasma confinement tube and the injection probe for the carrier gas) can be treated in a consistent manner and, accordingly, no fictitious terms need to be introduced in momentum and energy equations. Moreover, flow field equations are solved only inside the torch region. This results in an overall saving of computational time per single iteration with respect to the UDS method.

Besides that, as the UDF approach solves vector potential and flow field equations on separated grids, the dimensions of the extended EM field domain can be fixed independently from those of the fluid dynamic mesh. This represents a useful advantage, in particular when the flow field domain is greater than the torch region (*e.g.*, in the study of plasma-spray applications by means of models taking into account both the torch and plasma downstream zones).

4 Results and discussion

All the calculations have been carried out by means of the FLUENT© code for the torch geometry shown in Figure 1 (Tekna Plasma Systems Inc. PL-50 model); dimensions of the torch and operating conditions used in the simulations are given in Table 1. The discharge is assumed to be operated in argon at atmospheric pressure. The net power dissipated in the plasma, P, is 5 kW (even though the Tekna

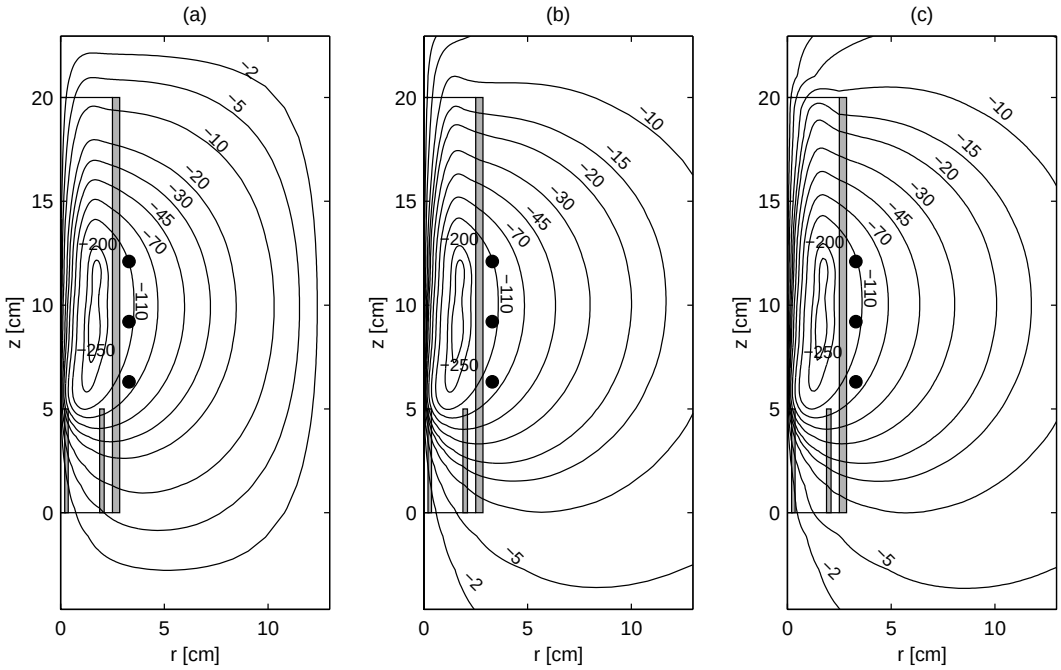

Fig. 3. Isocontours of the real part of the electric field [V/m] as obtained by means of the UDF technique within (a) EF and (b) MDBC approaches (radial dimension of the extended grid: $R_{\rm et} = 12.5$ cm) and within (c) ST approach for the EM field treatment.

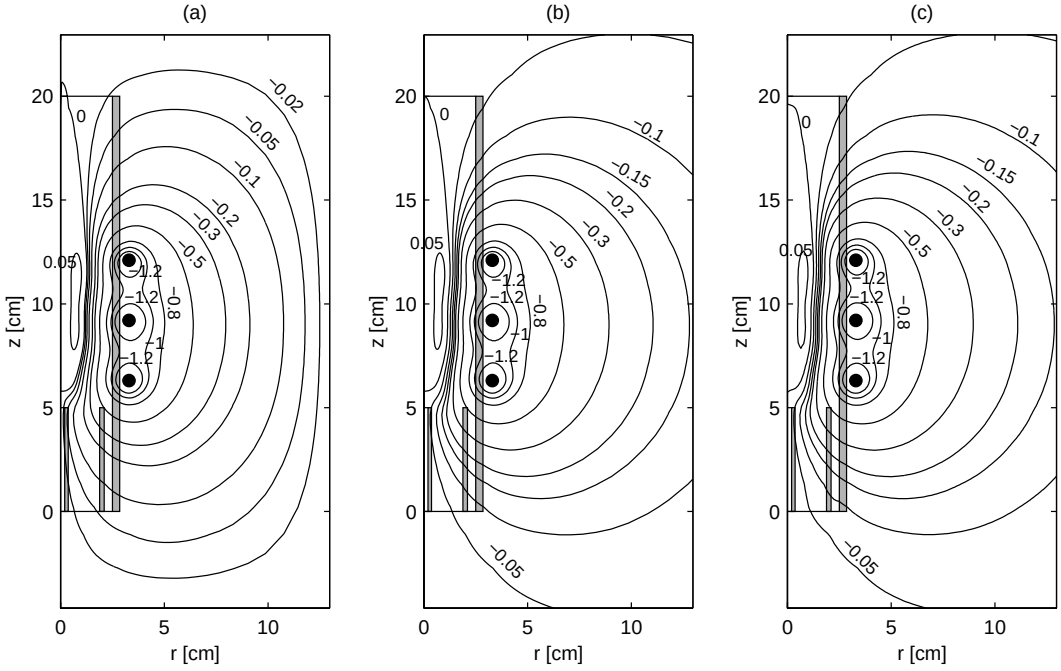

Fig. 4. Isocontours of the imaginary part of the electric field [10^3 V/m] as obtained by means of the UDF technique within (a) EF and (b) MDBC approaches (radial dimension of the extended grid: $R_{\rm et} = 12.5$ cm) and within (c) ST approach for the EM field treatment.

PL-50 plasma torch can be operated under much higher power conditions), while the RF generator frequency, f, is set at 3 MHz. Carrier, plasma and sheath gases are all injected axially in the torch (with flow rates Q_1, Q_2 and Q_3, respectively).

Figures 3 and 4 show the distributions of the real and imaginary parts of the electric field as calculated by means of the UDF technique, using the three above-mentioned approaches for the EM field treatment. For the EF and MDBC approaches, a non-uniform, structured grid with $81(r) \times 71(z)$ points has been employed for the solution of the vector potential equations, using a computational domain which extends outside the torch region both in the radial and axial directions (see Fig. 2a). The radial

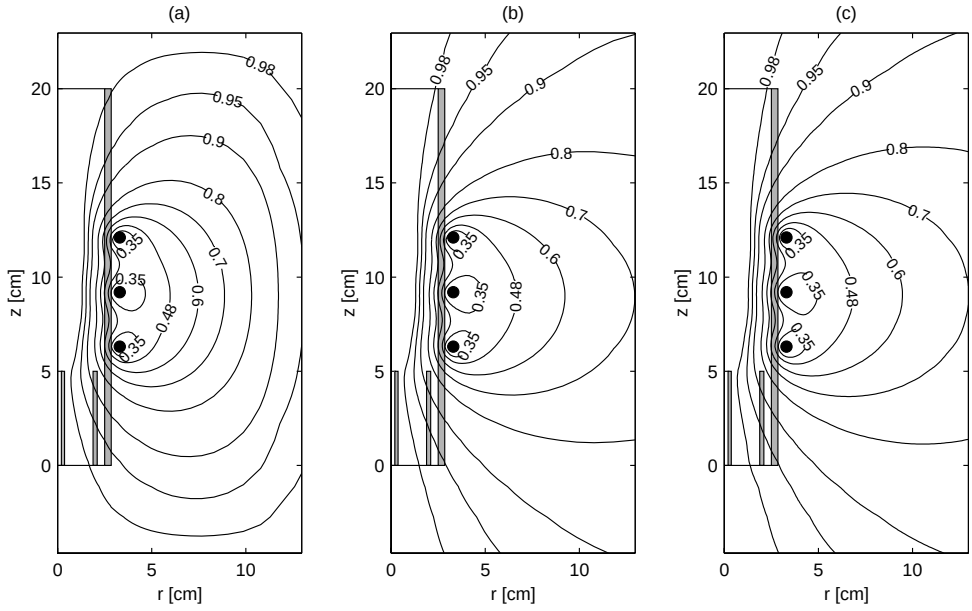

Fig. 5. Isocontours of the stream function of the real part of the magnetic field as obtained by means of the UDF technique within (a) EF and (b) MDBC approaches (radial dimension of the extended grid: $R_{\rm et} = 12.5$ cm) and within (c) ST approach for the EM field treatment. Minimum calculated values [T m^2]: (a), (b) -3.5×10^{-6}; (c) -3.4×10^{-6}. Maximum calculated values [T m^2]: (a), (b) 2.8×10^{-8}; (c) 2.6×10^{-8}. The results shown in this figure have been scaled to positive values and then normalized to unity.

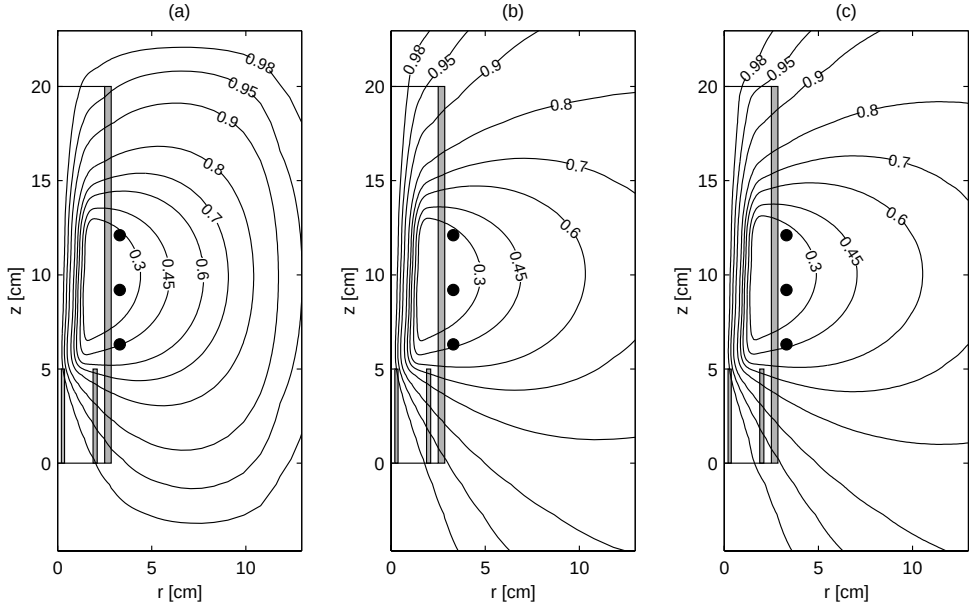

Fig. 6. Isocontours of the stream function of the imaginary part of the magnetic field as obtained by means of the UDF technique within (a) EF and (b) MDBC approaches (radial dimension of the extended grid: $R_{\rm et} = 12.5$ cm) and within (c) ST approach for the EM field treatment. Minimum and maximum calculated values for all three cases are: -2.6×10^{-7} T m^2 and 0.0, respectively. The results shown in this figure have been scaled to positive values and then normalized to unity.

dimension of the extended grid, $R_{\rm et}$, is 125 mm, corresponding to the value adopted in [10], while the boundaries of the domain in the axial direction are placed 47 mm and 30 mm away from the inlet and exit sections of the torch, respectively. A uniform, structured mesh with $57(r) \times 200(z)$ quadrilateral elements has been used for the fluid dynamic calculations in the torch zone. Within the ST approach, vector potential equations are solved in the plasma region only, on a grid which coincides with the fluid dynamic one, while the values of the electromagnetic field outside the discharge zone are determined at the end of the whole computation by means of the current-carrying loop formula, summing the contributions of the currents calculated in the plasma and of those flowing through the rings used to represent the induction coil (see Fig. 2a for the details of the coil discretization).

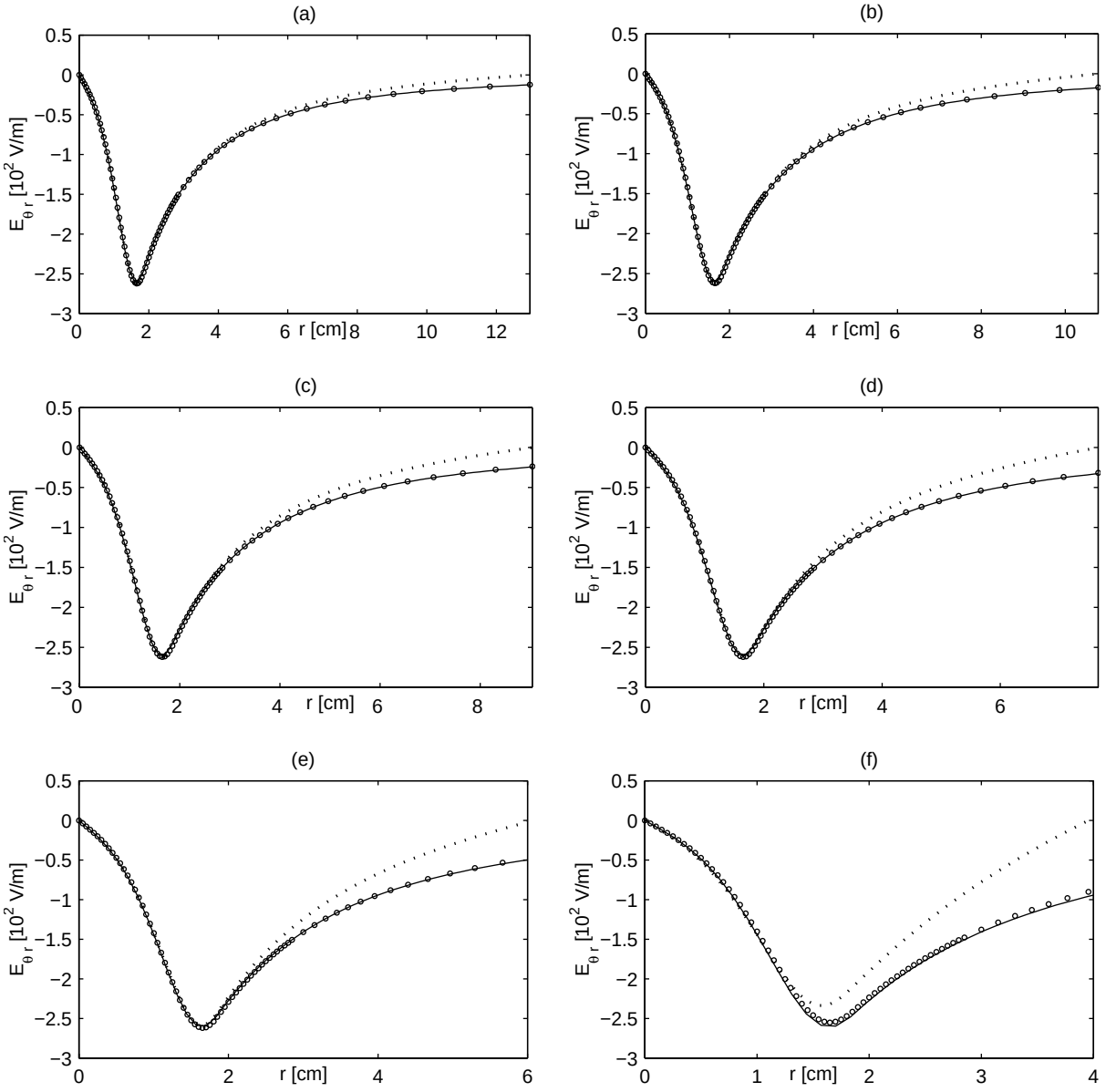

Fig. 7. Radial profiles of the real part of the electric field, $E_{\theta r}$, at $z = 10.2$ cm, as obtained by means of the UDF technique within ST approach (—) for the EM field treatment and within EF ($\cdots$) and MDBC ($\circ$) approaches with different radial extensions of the EM grid: $R_{\rm et} = 12.5$ cm (a); 11 cm (b); 9 cm (c); 7.5 cm (d); 6 cm (e); 4 cm (f).

Figures 3 and 4 clearly show that, although in the plasma region the distributions of the electric field obtained by the three different approaches considered here for the EM field treatment are nearly the same, the results given by the MDBC approach (Figs. 3b and 4b) far away from the torch zone are more precise than those calculated by the EF method (Figs. 3a and 4a), as demonstrated by the comparison of such results with the corresponding "exact" ones obtained by the ST model (Figs. 3c and 4c). This is due to the fact that, unlike the MDBC approach, the EF one imposes the vanishing of the electric field at finite distances from the torch, which is clearly not a realistic condition. The isocontours of the stream function of the real and imaginary parts of the corresponding magnetic fields are presented in Figures 5 and 6, respectively: the EF, MDBC and ST approaches still give the same results in the plasma and coil regions, while strong differences between the EF and MDBC models arise faraway from the torch zone. As expected, the comparisons of Figures 5a, 5b with Figure 5c and of Figures 6a, 6b with Figure 6c confirm that the MDBC approach is more precise than the EF one in describing the EM field outside the plasma region. Therefore, the use of the MDBC model might be helpful for those applications in which the prediction of the EM field distribution outside the torch zone is also important (*e.g.*, in the design of electromagnetic shields for RF plasma systems or for studying torches with ferrite around the coil [13,14]), as it combines the precision of the ST approach with the simplicity of the EF one.

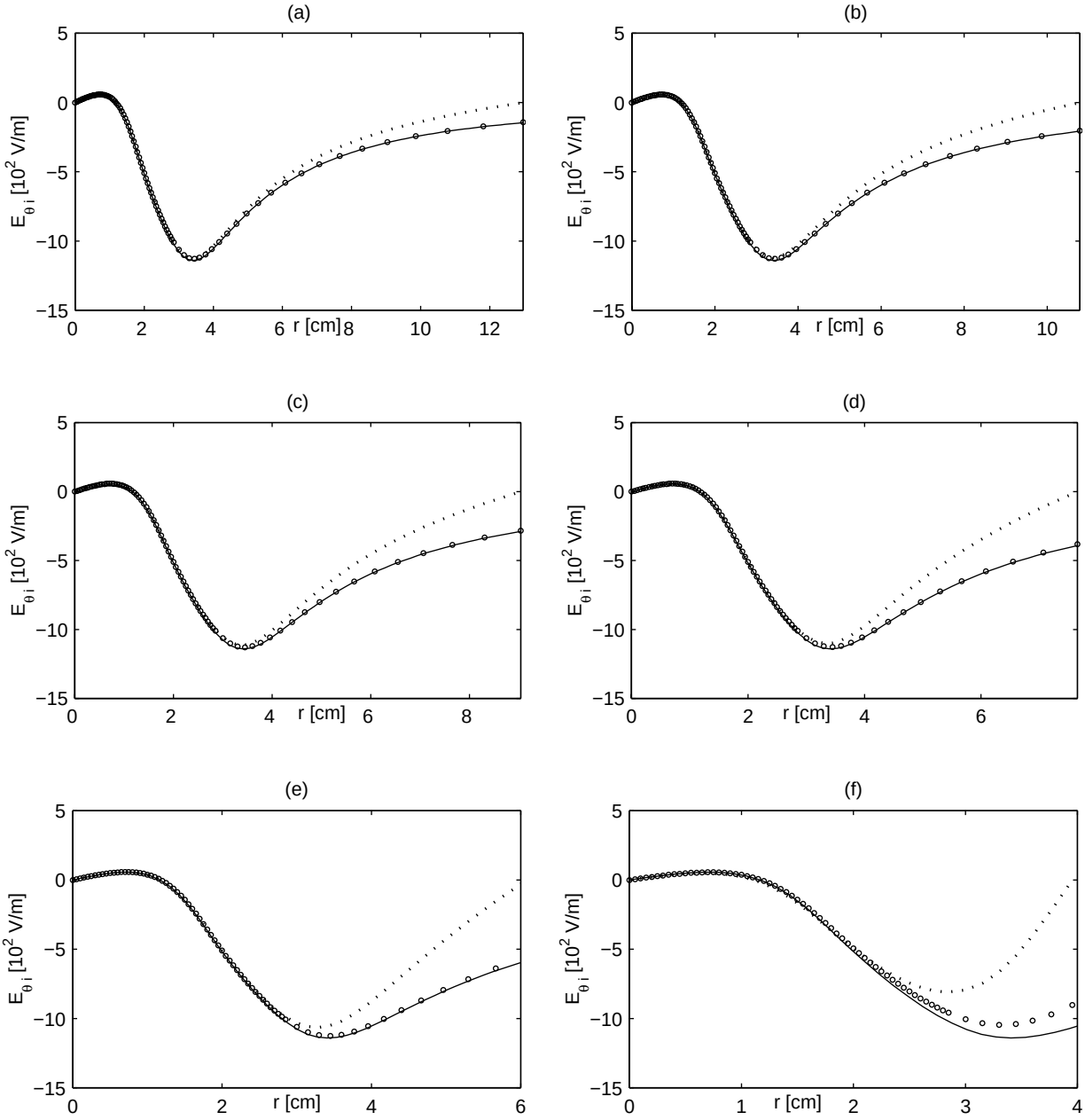

Fig. 8. Radial profiles of the imaginary part of the electric field, $E_{\theta \mathrm{i}}$, at $z = 10.2$ cm, as obtained by means of the UDF technique within ST approach (—) for the EM field treatment and within EF ($\cdots$) and MDBC ($\circ$) approaches with different radial extensions of the EM grid: $R_{\mathrm{et}} = 12.5$ cm (a); 11 cm (b); 9 cm (c); 7.5 cm (d); 6 cm (e); 4 cm (f).

Moreover, the MDBC approach permits a decrease of the dimension of the extended grid, so reducing the computational effort, while still guaranteeing a good precision of the solution in the zone extending outside the discharge region as well. This is well evidenced in Figures 7 and 8, which show the radial profiles of the real and imaginary parts of the electric field, respectively, at $z = 102$ mm, as calculated by the ST model and by the EF and MDBC approaches, for different radial dimensions of the extended domain. For each value of R_{et} considered, the number of discretization points in the r-direction has been suitably chosen, so to keep the step sizes of the EM grid constant. The different spacing between points appearing in the MDBC curves is due to the non-uniformity of the mesh. For $R_{\mathrm{et}} = 125$ mm, all approaches for treating the EM field give almost the same results. However, as the radial extension of the grid is reduced, the behaviour of the electric field obtained by the EF approach in the region extending outside the torch domain differs more and more from those calculated by

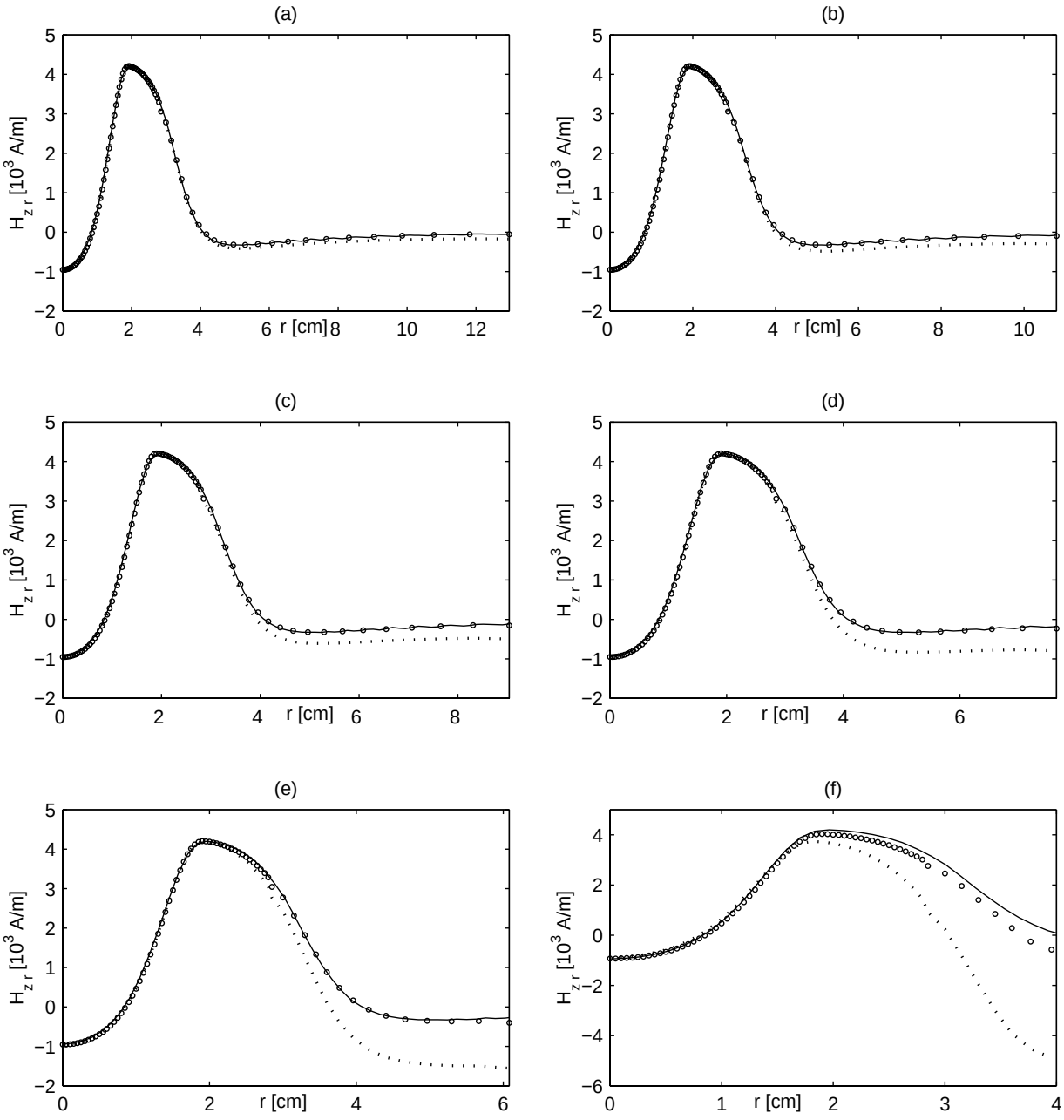

Fig. 9. Radial profiles of the real part of the axial magnetic field, H_{zr}, at $z = 10.2$ cm, as obtained by means of the UDF technique within ST approach (—) for the EM field treatment and within EF ($\cdots$) and MDBC ($\circ$) approaches with different radial extensions of the EM grid: $R_{\rm et} = 12.5$ cm (a); 11 cm (b); 9 cm (c); 7.5 cm (d); 6 cm (e); 4 cm (f).

the ST and MDBC ones, since the vector potential near the coil zone is considerably different from zero. On the contrary, the MDBC approach continues to give acceptable results also for small extensions of the grid outside the torch region. For $R_{\rm et} < 60$ mm, the electric field calculated by means of the EF approach starts to deviate from the solution obtained by the other two approaches also inside the plasma zone, as demonstrated by Figures 11 and 12, which show the axial profiles of the real and imaginary parts of the electric field at the inner surface of the plasma confinement tube, for the same cases as Figures 7 and 8. A similar behaviour can be observed also for the magnetic field, as shown in Figures 9, 10 and in Figures 13, 14, in which the same kinds of results as Figures 7, 8 and 11, 12 are presented.

In order to validate the new UDF technique proposed in this work, the radial profiles of the electric and magnetic fields for the case of the EF approach with $R_{\rm et} = 125$ mm (see Figs. 7a, 8a and 9a, 10a) have been compared to the corresponding literature results [10] obtained by Boulos

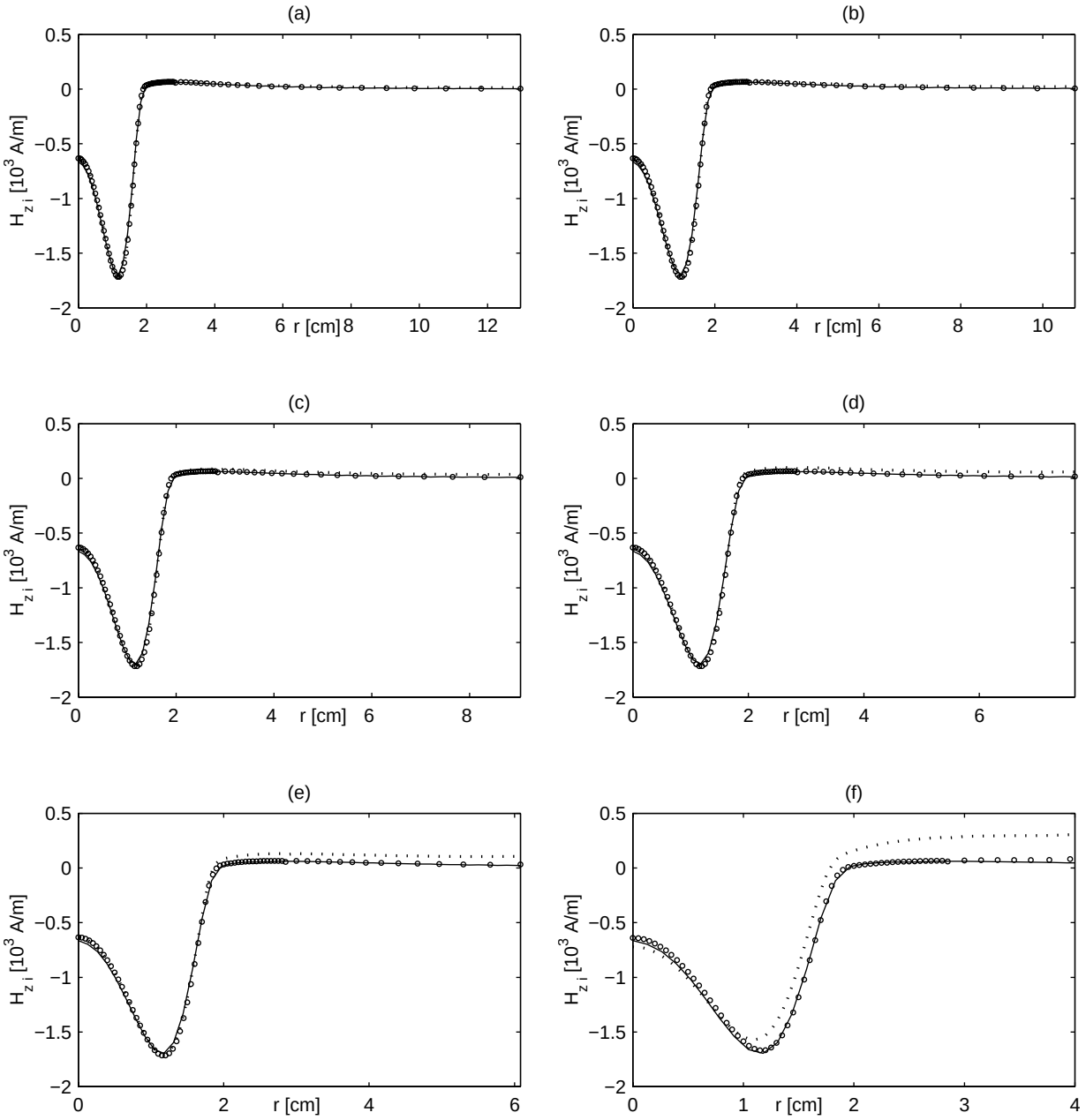

Fig. 10. Radial profiles of the imaginary part of the axial magnetic field, H_{zi}, at $z = 10.2$ cm, as obtained by means of the UDF technique within ST approach (—) for the EM field treatment and within EF ($\cdots$) and MDBC ($\circ$) approaches with different radial extensions of the EM grid: $R_{\mathrm{et}} = 12.5$ cm (a); 11 cm (b); 9 cm (c); 7.5 cm (d); 6 cm (e); 4 cm (f).

et al. using the UDS technique. A computational grid extending outside the torch region only in the radial direction was adopted in [10], assuming $R_{\mathrm{et}} = 125$ mm. The comparisons show a full agreement for both real and imaginary parts of the EM field profiles, also proving that extending the computational domain beyond the torch zone in the axial direction has a minor impact on the calculated EM field distribution in the central region of the discharge.

A selection of results obtained by the MDBC approach for the case with $R_{\mathrm{et}} = 125$ mm are presented in Figures 15, 16, 17 and 18, showing isocontours of temperature field, stream function velocity, power density distribution and radial component of the Lorentz force in the plasma, respectively, along with the profiles of plasma temperature and axial velocity along the centerline of the torch (Fig. 19). Essentially the same behaviour can be seen with regard to the EF and ST models. A good agreement can be

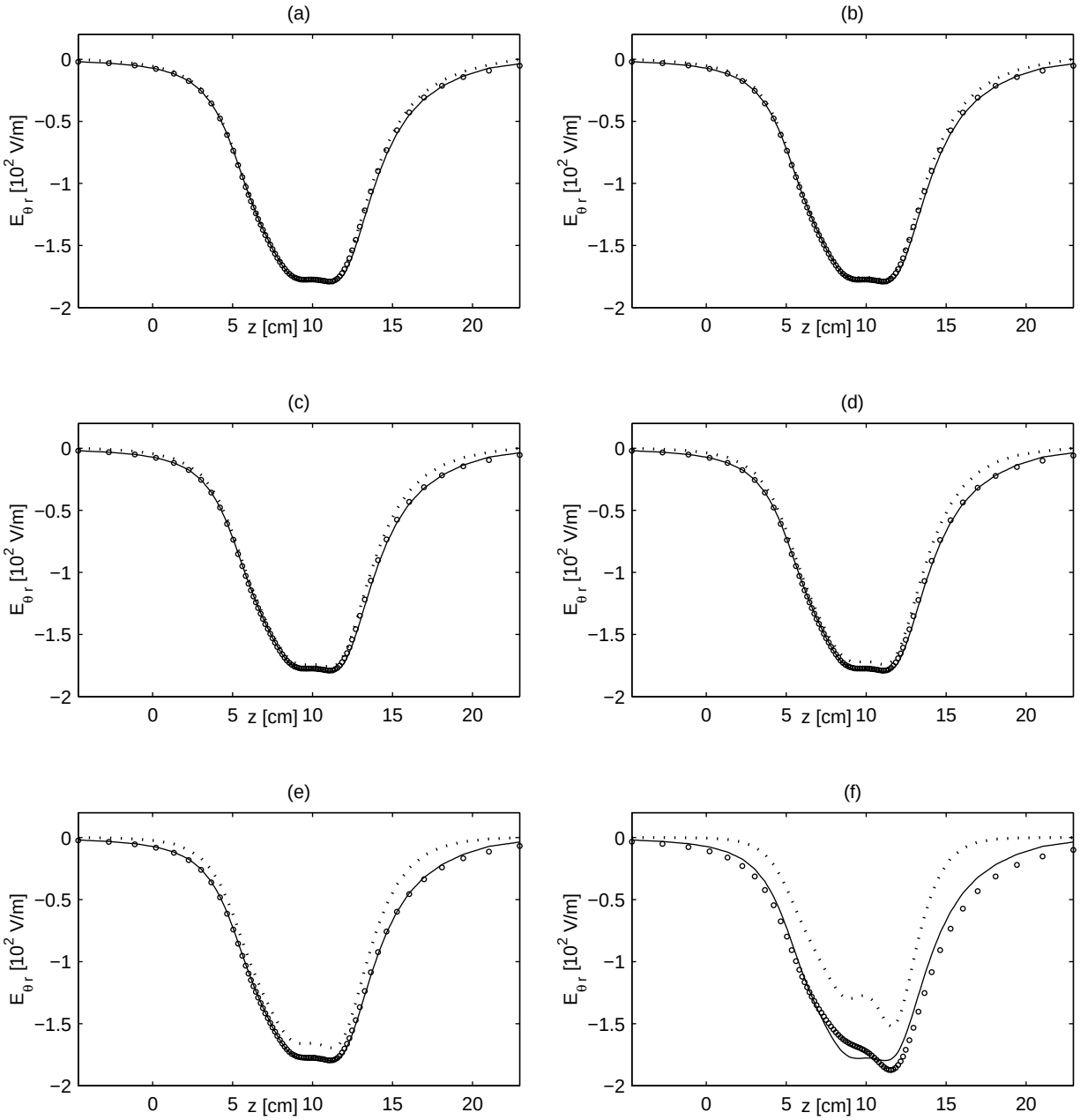

Fig. 11. Axial profiles of the real part of the electric field, $E_{\theta \mathrm{r}}$, at the inner wall of the plasma confinement tube ($r = 2.5$ cm), as obtained by means of the UDF technique within ST approach (—) for the EM field treatment and within EF ($\cdots$) and MDBC ($\circ$) approaches with different radial extensions of the EM grid: $R_{\mathrm{et}} = 12.5$ cm (a); 11 cm (b); 9 cm (c); 7.5 cm (d); 6 cm (e); 4 cm (f).

observed between these results and those calculated in [10] for the same torch dimensions and operating conditions, but using the UDS technique within the EF approach. This is actually what one would expect, as the boundary of the extended grid in the radial direction is taken far enough from the torch zone to obtain consistent solutions between the two approaches (EF and MDBC) employed for the EM field calculations. In our UDF-MDBC simulation, the coil current needed to sustain the 5 kW plasma discharge is 150 A, which is in acceptable agreement with the value of 161 A reported in [10].

In order to evaluate the performances of our new UDF technique, the calculations carried out by means of such technique for the case of the EF approach with $R_{\mathrm{et}} = 125$ mm, have been accomplished using also the UDS method, following what was done in [10]. In our case, a structured grid with quadrilateral elements has been employed inside the torch region, while an unstructured

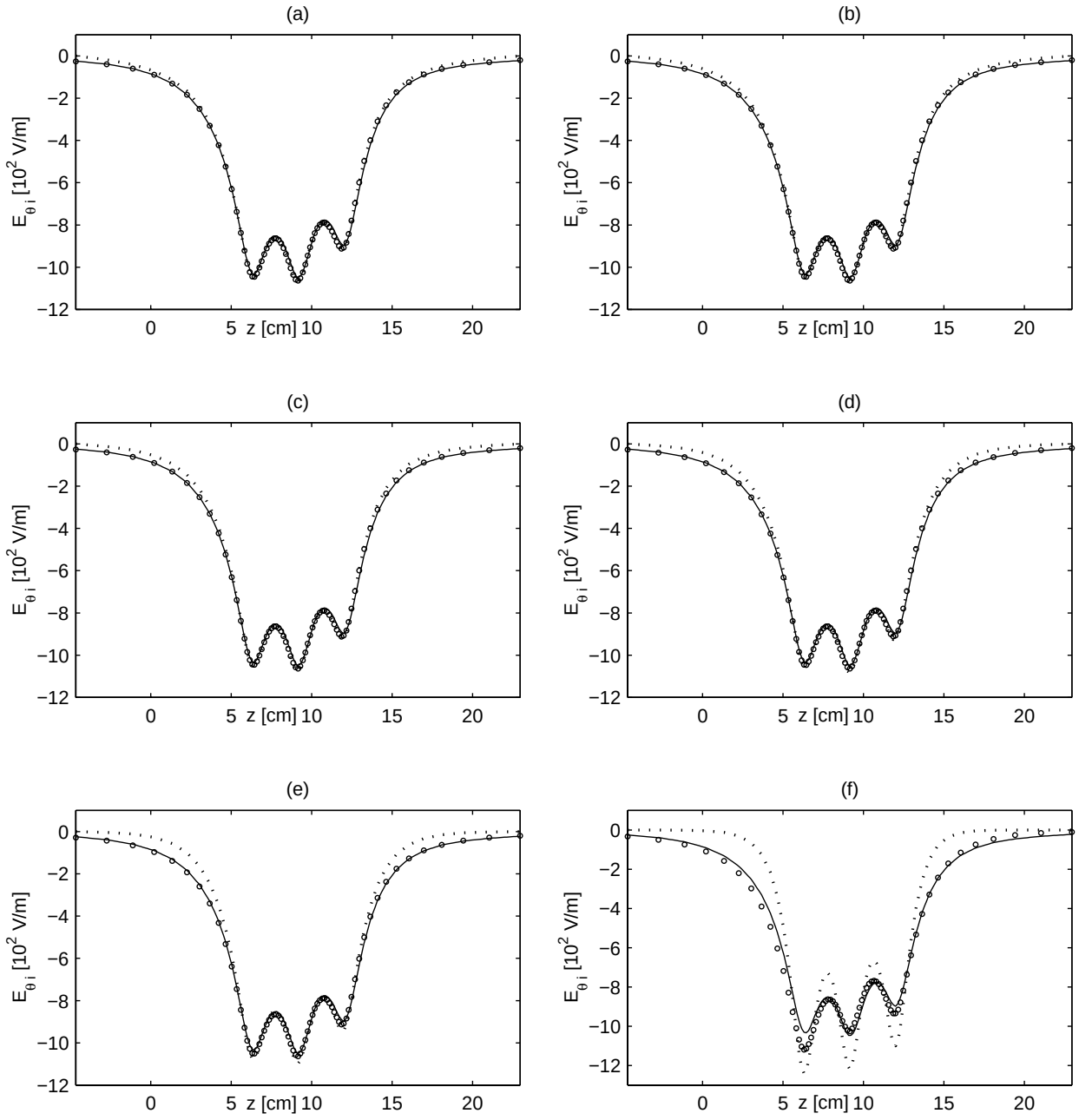

Fig. 12. Axial profiles of the imaginary part of the electric field, $E_{\theta i}$, at the inner wall of the plasma confinement tube ($r = 2.5$ cm), as obtained by means of the UDF technique within ST approach (—) for the EM field treatment and within EF ($\cdots$) and MDBC ($\circ$) approaches with different radial extensions of the EM grid: $R_{et} = 12.5$ cm (a); 11 cm (b); 9 cm (c); 7.5 cm (d); 6 cm (e); 4 cm (f).

mesh with triangular cells, extending outside the plasma zone only in the radial direction, has been adopted (see Fig. 2b). Figure 20 shows the comparison between the computational time over one single iteration required by the two techniques: asymptotic values of about 1 and 0.4 s have been obtained for the UDS and UDF approaches, respectively; this proves that the latter is characterized by better performances, as a result of the fact that fluid dynamic equations are solved only in the torch domain.

5 Conclusions

In this paper, a new technique has been developed for numerically simulating the behaviour of inductively coupled

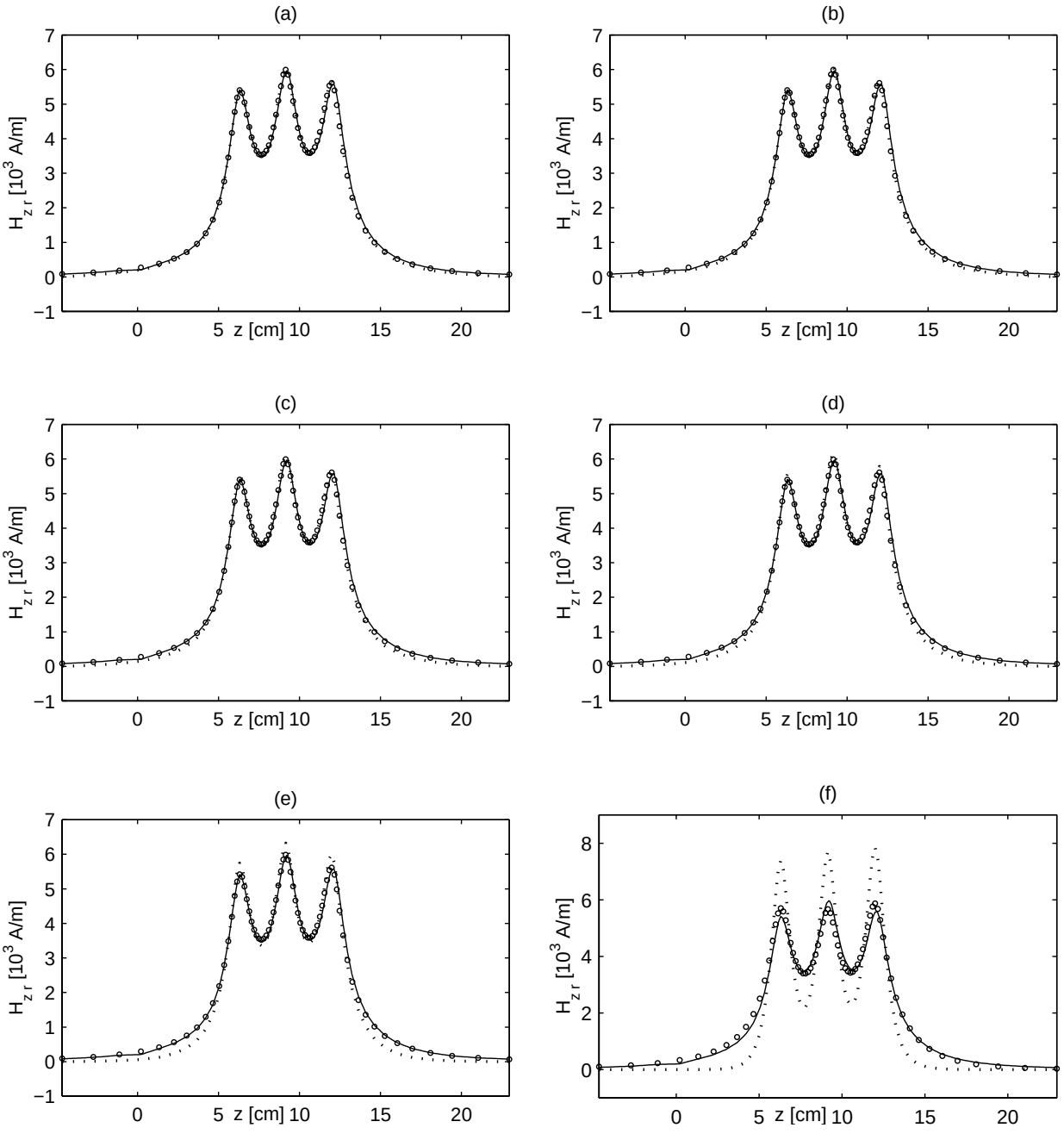

Fig. 13. Axial profiles of the real part of the axial magnetic field, H_{zr}, at the inner wall of the plasma confinement tube ($r = 2.5$ cm), as obtained by means of the UDF technique within ST approach (—) for the EM field treatment and within EF ($\cdots$) and MDBC ($\circ$) approaches with different radial extensions of the EM grid: $R_{et} = 12.5$ cm (a); 11 cm (b); 9 cm (c); 7.5 cm (d); 6 cm (e); 4 cm (f).

plasma torches by means of the CFD commercial code FLUENT©.

Unlike the method previously proposed in the literature, which employed user-defined scalars for the real and imaginary parts of the vector potential in addition to the variables basically used by the commercial software to describe fluid temperature and velocity, the new technique presented here consists of a linked external function which completely solves the electromagnetic field equations, while letting the FLUENT© built-in module calculate only temperature and flow fields inside the torch region. Computations carried out by using both techniques have proved that the new one converges faster and also eliminates some numerical problems which could arise using the method based on user-defined scalars.

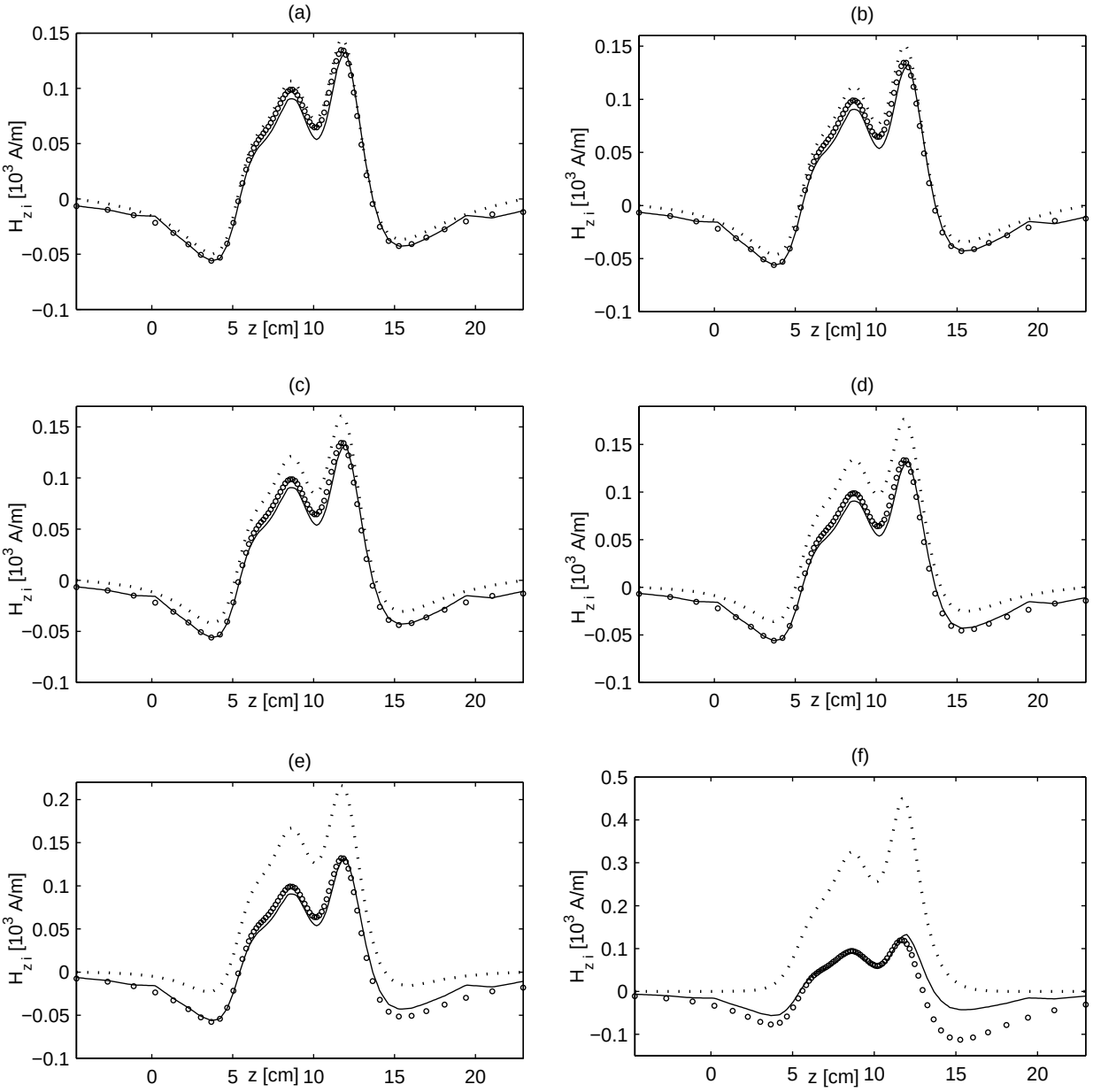

Fig. 14. Axial profiles of the imaginary part of the axial magnetic field, H_{zi}, at the inner wall of the plasma confinement tube ($r = 2.5$ cm), as obtained by means of the UDF technique within ST approach (—) for the EM field treatment and within EF ($\cdots$) and MDBC ($\circ$) approaches with different radial extensions of the EM grid: $R_{et} = 12.5$ cm (a); 11 cm (b); 9 cm (c); 7.5 cm (d); 6 cm (e); 4 cm (f).

Different approaches for the treatment of the electromagnetic field have been implemented within the new FLUENT©-based technique described in this work. In particular, the results obtained by using both magnetic dipole and vanishing boundary conditions in the framework of an EM extended grid model have been compared with those given by the standard approach, based on exact integral boundary conditions for the vector potential. The comparisons show that, although for sufficient extension of the electromagnetic grid outside the torch region the two methods produce essentially the same solution, for small radial dimensions of the mesh outside the plasma zone, the magnetic dipole approach is more precise than that using vanishing vector potential conditions.

Future developments will lie in the use of the UDF technique also in conjunction with the FLUENT© built-in models for the study of turbulent fluid dynamic regimes in the torch. The authors believe, also on the basis of some preliminary tests, that the UDF method should greatly reduce the numerical instabilities associated to the solution

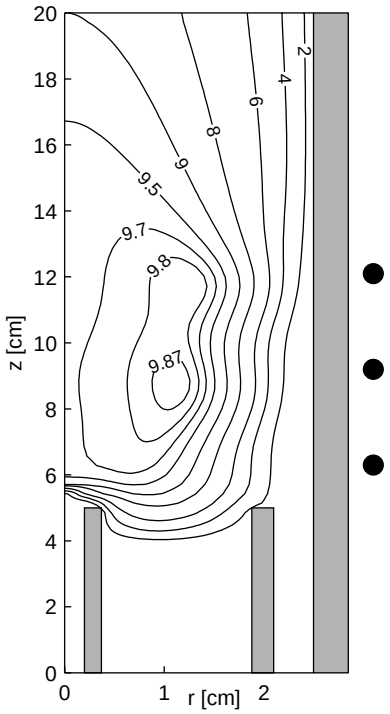

Fig. 15. Plasma temperature field [10^3 K] as obtained by means of the UDF technique within MDBC approach for the EM field treatment with $R_{\rm et} = 12.5$ cm.

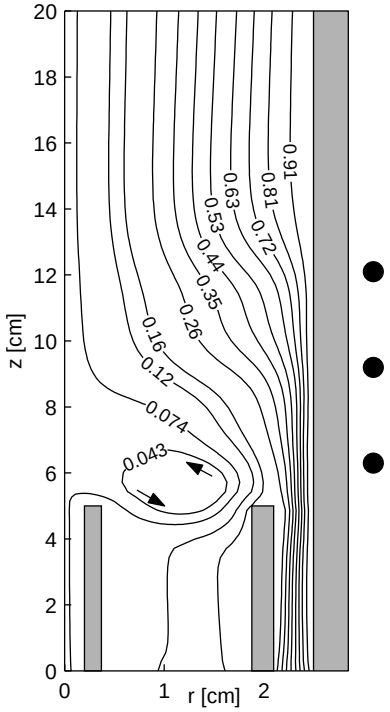

Fig. 16. Isocontours of the stream function of the plasma velocity as obtained by means of the UDF technique within MDBC approach for the EM field treatment with $R_{\rm et} = 12.5$ cm. Minimum calculated value: -1.14×10^{-5} kg/s; maximum calculated value: 1.52×10^{-4} kg/s. The results shown in this figure have been scaled to positive values and then normalized to unity.

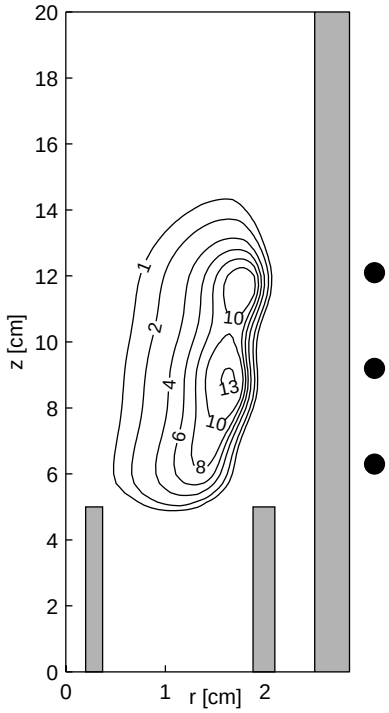

Fig. 17. Power density distribution [10^7 W/m^3] in the plasma, as obtained by means of the UDF technique within MDBC approach for the EM field treatment with $R_{\rm et} = 12.5$ cm.

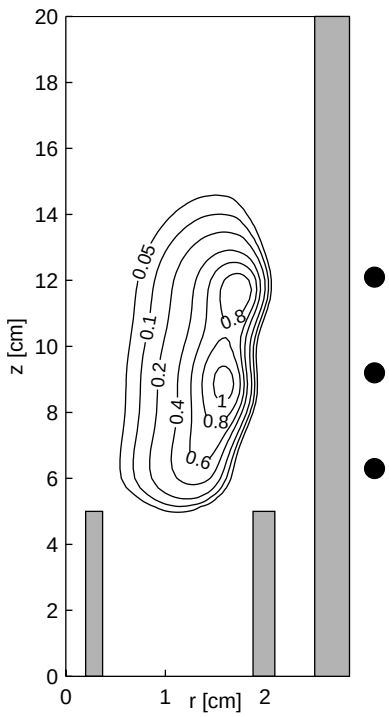

Fig. 18. Radial component of the Lorentz force ($-F_r$) [10^3 N/m^3], as obtained by means of the UDF technique within MDBC approach for the EM field treatment with $R_{\rm et} = 12.5$ cm.

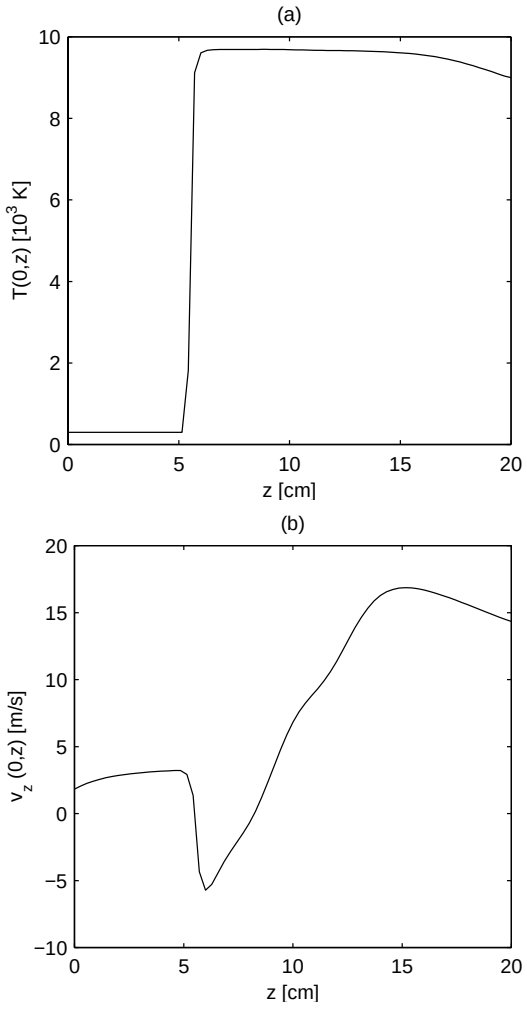

Fig. 19. Axial profiles of (a) plasma temperature and (b) axial velocity along the centerline of the torch, as obtained by means of the UDF technique within MDBC approach for the EM field treatment with $R_{\rm et} = 12.5$ cm.

of turbulence equations, which tend to arise when using the UDS approach as a consequence of treating all regions of the computational domain as a fluid.

This work was performed with partial financial support from the National Group for Mathematical Physics (G.N.F.M.) of the Italian Institute of High Mathematics, from the University of Bologna goal-oriented projects 1999-2001 and 2001-2003, ex-60% 2001-2002 projects, and from the Italian Ministry of Education, University and Scientific Research (M.I.U.R.) national project COFIN 2002.

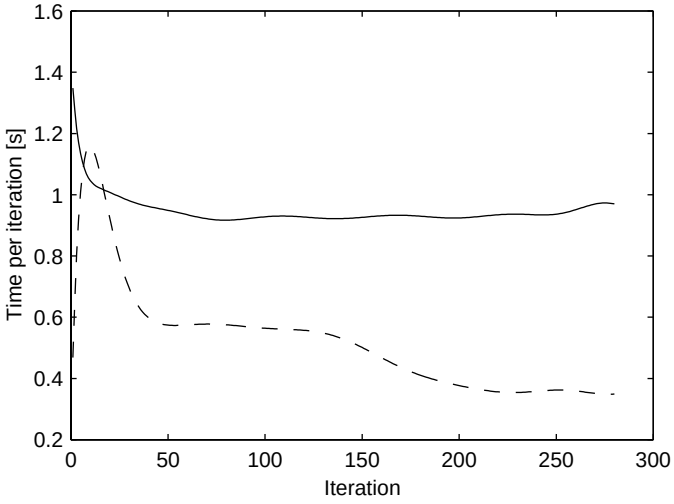

Fig. 20. Computational time over one single iteration required by (—) UDS and (- - -) UDF techniques within EF approach for the EM field treatment with $R_{\rm et} = 12.5$ cm.

References

1. D. Bernardi, V. Colombo, E. Ghedini, A. Mentrelli, in *Atti del XVI Congresso dell'Associazione Italiana del Vuoto, Catania (Italy), 7-9 October 2002*, edited by Editrice Compositori (Bologna, 2003), pp. 267–272
2. D. Bernardi, V. Colombo, E. Ghedini, A. Mentrelli, Eur. Phys. J. D **22**, 119 (2003)
3. R. Ye, P. Proulx, M.I. Boulos, Int. J. Heat Mass Trans. **42**, 1585 (1999)
4. S. Xue, P. Proulx, M.I. Boulos, Plasma Chem. Plasma Process. **23**, 245 (2003)
5. X. Chen, J. Phys. D: Appl. Phys. **22**, 361 (1989)
6. J. Mostaghimi, M.I. Boulos, Plasma Chem. Plasma Process. **9**, 25 (1989)
7. X. Chen, E. Pfender, Plasma Chem. Plasma Process. **11**, 103 (1991)
8. V. Colombo, C. Panciatichi, A. Zazo, G. Cocito, L. Cognolato, IEEE Trans. Plasma Sci. **25**, 1073 (1997)
9. D. Bernardi, V. Colombo, G.G.M. Coppa, A. D'Angola, Eur. Phys. J. D **14**, 337 (2001)
10. S. Xue, P. Proulx, M.I. Boulos, J. Phys. D: Appl. Phys. **34**, 1897 (2001)
11. J.D. Jackson, *Classical Electrodynamics*, 2nd edn. (Wiley, New York, 1975), pp. 219–223
12. R.C. Miller, R.J. Ayen, J. Appl. Chem. **40**, 5260 (1969)
13. S. Xue, P. Proulx, M.I. Boulos, J. Phys. D: Appl. Phys. **35**, 1123 (2002)
14. S. Xue, P. Proulx, M.I. Boulos, J. Phys. D: Appl. Phys. **35**, 1131 (2002)